

AI-based automated framework for quantitative PET/CT image analysis

Sonja Adomeit, Lukas Förner, Elisabeth Scheurer, Jan Bäßler, Elina Gastreich de Llanes, Jonas Böhringer, Ralph A. Bundschuh, Constantin Lapa, Kartikay Tehlan, Thomas Wendler

Angaben zur Veröffentlichung / Publication details:

Adomeit, Sonja, Lukas Förner, Elisabeth Scheurer, Jan Bäßler, Elina Gastreich de Llanes, Jonas Böhringer, Ralph A. Bundschuh, Constantin Lapa, Kartikay Tehlan, and Thomas Wendler. 2026. "AI-based automated framework for quantitative PET/CT image analysis." In *Bildverarbeitung für die Medizin 2026: proceedings, German Conference on Medical Image Computing, Lübeck, March 15-17, 2026*, edited by Heinz Handels, Katharina Breininger, Thomas Deserno, Andreas Maier, Klaus Maier-Hein, Christoph Palm, and Thomas Tolxdorff, 139–45. Wiesbaden: Springer Fachmedien.
https://doi.org/10.1007/978-3-658-51100-5_30.



AI-based Automated Framework for Quantitative PET/CT Image Analysis

Sonja Adomeit ^{1,2†}, Lukas Förner ^{1,2,3†}, Elisabeth Scheurer⁴, Jan Bäßler ⁴,
Elina Gastreich de Llanes ^{1,2}, Jonas Böhringer^{1,2}, Ralph A. Bundschuh ⁵,
Constantin Lapa ^{4,6}, Kartikay Tehlan ^{1,2,3}, Thomas Wendler ^{1,2,3,6,7}

¹Department of Diagnostic and Interventional Radiology and Neuroradiology, University Hospital Augsburg

²Digital Medicine, University Hospital Augsburg

³Computer-Aided Medical Procedures and Augmented Reality, Technical University of Munich

⁴Department of Nuclear Medicine, University Hospital Augsburg

⁵Department of Nuclear Medicine, University Hospital Carl Gustav Carus

⁶Bavarian Cancer Research Center (BZKF) Augsburg

⁷Center of Advanced Analytics and Predictive Sciences, University of Augsburg
sonja.adomeit@med.uni-augsburg.de

Abstract. Radiomics extracts quantitative features from medical images, offering biomarkers for diagnosis, prognosis, and evaluation of treatment response. Yet, its broader application in research is limited by the absence of standardized, end-to-end workflows for multimodal imaging. We present an open-source Python-based pipeline that allows for interactive studies and series selection, as well as automated conversion, segmentation, and quantitative analysis of positron emission tomography (PET) / computed tomography (CT) DICOM images. Leveraging widely adopted segmentation models for PET analysis and CT organ delineation, the pipeline computes key radiomics, producing structured outputs for analysis. Its modular design facilitates reproducible, scalable, and clinically relevant radiomics studies, addressing a critical gap in medical image analysis infrastructure. The code is available under: <https://github.com/Clinical-Computational-Medical-Imaging/MUSIQ>

1 Introduction

The digitization of medical imaging and the rise of artificial intelligence (AI) have transformed clinical research and are increasingly supporting daily practice [1]. Within this broader context, radiomics computationally derives quantitative descriptors from medical images, capturing intensity patterns, spatial relationships, and structural properties beyond visual assessment [2, 3]. These feature sets are applied

[†]These authors contributed equally to this work.

across imaging modalities and diseases, showing promise for linking image data with disease biology and clinical outcomes [4, 5].

Despite its potential, the adoption of radiomics in clinical data science is hindered by the lack of standardized, end-to-end workflows [6, 7]. Conventional workflows depend on separate tools for data handling, preprocessing, segmentation, and feature extraction, each with distinct dependencies and formats. The lack of integration increases manual effort, variability, and limits reproducibility. Although tools like `matRadiomics` [8], `LIFEx` [9], and `CERR` [10] particularly aid non-programmers in radiomics extraction and analysis, their focus on graphical user interfaces makes them less suited for seamless integration into deep learning pipelines for advanced data science.

By integrating complementary anatomical and functional data, PET/CT is particularly well-suited for combined quantitative analysis [11]. Therefore, we present an open-source, Python-based pipeline for PET/CT radiomics extraction to address a critical gap in reproducible, scalable, and extensible radiomics research infrastructure.

2 Materials and methods

The following section outlines each step of the proposed pipeline (Fig. 1).

2.1 Data preparation and initialization

Relevant imaging series are selected from the digital imaging and communications in medicine (DICOM) directory using user-defined keywords or via manual selection. Alignment of PET and CT images is required. DICOM files are converted to neuroimaging informatics technology initiative (NIfTI) format. For PET data, voxel intensities are expressed as standardized uptake value (SUV) normalized by injected dose, physical decay, and patient body weight. Patient data are parsed from DICOM metadata and structured in JSON format.

2.2 Segmentation

The pipeline supports automated segmentation for functional and anatomical imaging using widely adopted open-source models. PET lesion masks are generated from SUV-normalized PET volumes with `autoPET3` [12]. Anatomical segmentation of CT data is performed with `TotalSegmentator` [13] and `Moose` [14, 15], enabling organ and skeletal delineation. Outputs are stored as NIfTI masks with accompanying metadata, including model, software version, and execution parameters.

2.3 Radiomics extraction

Computed radiomics metrics cover lesion-wise PET intensity, whole-body tumor burden, morphological and dissemination descriptors, as well as CT-based measurements.

For each patient, we first derive conventional SUV-based PET metrics: SUV_{max} (highest voxel intensity), SUV_{mean} (mean SUV), and SUV_{peak} , which we define as the median SUV in a fixed 1 cm^3 cubic region centered on the hottest voxel (peak-ROI definitions vary across studies) [16, 17]. Lesion metabolic tumor volume (MTV) is obtained as the volume of all voxels exceeding either an absolute SUV threshold (2.5–4.0) [18] or a relative threshold (30–50% of SUV_{max}) [19].

To capture whole-body disease burden, we aggregate lesion-wise metrics. The total metabolic tumor volume (TMTV) is defined as the combined volume of all segmented lesions [20]. Total lesion activity (TLA) is computed as SUV_{mean} multiplied by the corresponding lesion volume and summed over all lesions [21].

Morphological descriptors are derived from the binary lesion mask. The lesion count equals the number of spatially distinct connected components. Individual and total lesion volumes are computed by summing the physical voxel volumes of the respective components. Surface area is estimated from the isosurface of the binary mask using a marching-cubes approach with correct voxel spacing [22]. Tumor dissemination (D_{max}) is quantified as the maximum 3D Euclidean distance between any two lesion voxels and can be standardized by patient anthropometrics (SD_{max}) [23]. Organ overlap ratios are obtained by intersecting the lesion mask with predefined organ segmentations [7].

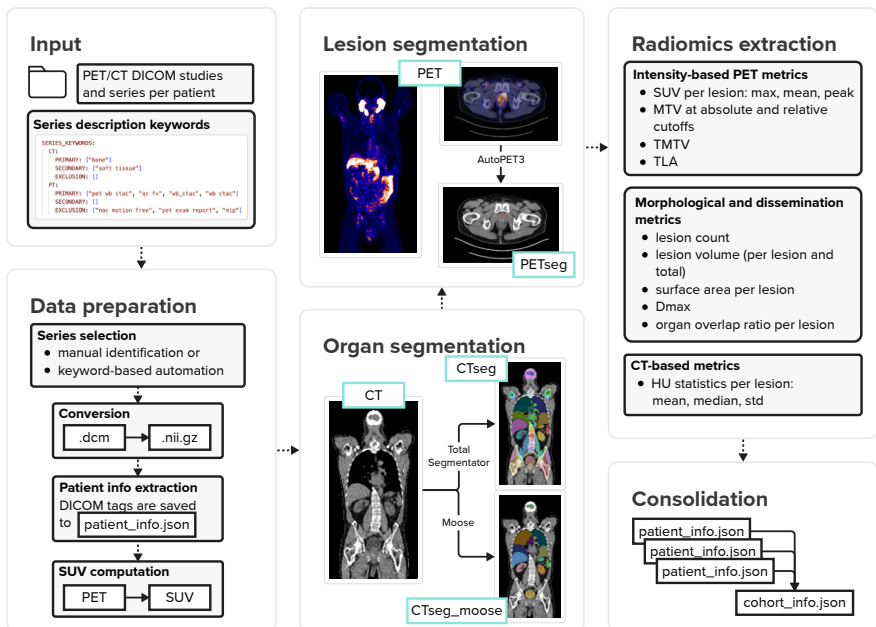


Fig. 1. Workflow visualization from data input to result consolidation. Dotted lines indicate workflow order, solid lines denote conversion/computation. Turquoise boxes describe the data modality of example images.

Finally, for each PET-defined lesion, we extract CT-based intensity statistics (mean, median, standard deviation of Hounsfield units) from the corresponding CT region to enable joint PET/CT analyses.

3 Results

The following case studies illustrate practical applications of the presented pipeline.

3.1 Automated PSMA-PET-based tumor quantification in prostate cancer and its association with Gleason score

We retrospectively analyzed in-house prostate-specific membrane antigen (PSMA) PET/CT scans from 369 patients with histologically confirmed prostate cancer to evaluate the relationship between PET-derived metrics and histopathological aggressiveness. The median and mean Gleason scores were 7.0 and 7.63, respectively. Spearman correlation analysis between Gleason scores and all pipeline-computed radiomics revealed that MTV at thresholds 4.0 ($\rho = 0.416$), 3.5 ($\rho = 0.406$), 3.0 ($\rho = 0.399$), 2.5 ($\rho = 0.397$), and TLA ($\rho = 0.403$) showed the strongest positive correlations ($p < 0.001$), suggesting a significant positive association between metabolic tumor burden and aggressiveness (Fig. 2).

3.2 AI-based FDG PET/CT analysis for immunotherapy response in metastatic melanoma

The pipeline was evaluated on 76 patients with metastatic melanoma undergoing immunotherapy. Baseline and follow-up fluorodeoxyglucose (FDG) PET/CT images were processed automatically and compared with manual segmentations by a nuclear

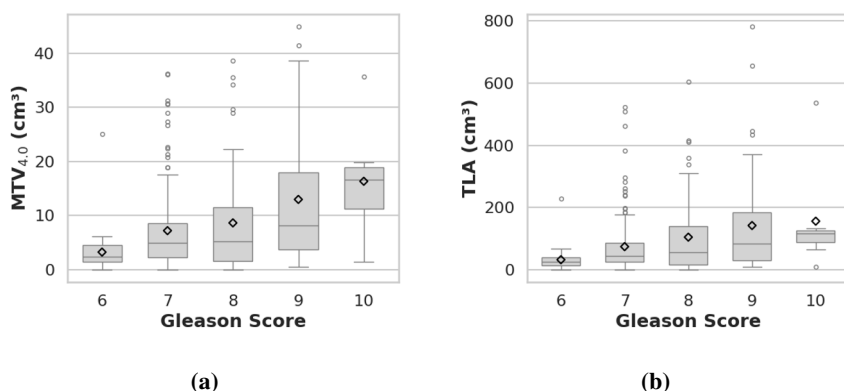


Fig. 2. MTV_{4.0} (a) and TLA (b) across Gleason scores, with \diamond indicating mean values. Data points exceeding 1.5 times the interquartile range were excluded for visual clarity.

medicine expert. AI segmentations showed good agreement with manual annotations, particularly for SUV_{max} , TMTV, and TLA ($R^2 = 0.86\text{--}0.89$), while discrepancies in D_{max} reflected methodological differences: manual measurements were taken on coronal maximum intensity projection images, while AI calculated 3D maximal distance between tumor voxels. Changes in automatically derived metrics between baseline and follow-up images corresponded well with clinical outcomes (stable disease, partial metabolic response, mixed response, progressive disease) and were consistent with lymph node dissection results [24].

4 Discussion

We present an open-source, Python-based pipeline for standardized PET/CT radiomics analysis, addressing the current lack of integrated workflows for radiomics computation in advanced data science. The pipeline is evaluated in two case studies using different tracers (PSMA, FDG), yielding results deemed clinically plausible.

Future developments will focus on expanding functionality, improving interoperability, and facilitating research adoption, as well as evaluating the robustness on further real-world clinical datasets. Planned enhancements include the incorporation of additional radiomics feature sets – such as PERCIST [16] metrics, texture features, and multiorgan-derived markers – and expanded segmentation models for both functional and anatomical imaging, along with meaningful visualizations. Beyond PET/CT, the pipeline’s modular design allows extension to other imaging modalities, including MRI and alternative PET tracers beyond FDG and PSMA, enabling more comprehensive multi-parametric analyses. To facilitate community use and collaboration, the framework will be released as an open-source Python package. Together, these improvements will strengthen the pipeline’s role as a scalable and extensible framework for radiomics research and its translation into clinical practice.

By combining robust processing, flexible integration, and a pathway for continuous expansion, this pipeline lays the foundation for reproducible, multimodal radiomics analyses that can accelerate digital medicine.

Acknowledgement. This research was partially funded by the Intramural Research Funding “MultiPro” of the Faculty of Medicine, University of Augsburg, the Bavarian Center for Cancer Research as part of the Lighthouse “Local Therapies”, as well as by the Bavarian Ministry of Economic Affairs, Regional Development and Energy (StMWi) under grant number DIK-2310-0004// DIK0556/02.

References

1. Alowais SA, Alghamdi SS, Alsuhebany N, Alqahtani T, Alshaya AI, Almohareb SN et al. Revolutionizing healthcare: the role of artificial intelligence in clinical practice. *BMC Med Educ.* 2023;23(1):689.

2. Lambin P, Rios-Velazquez E, Leijenaar R, Carvalho S, van Stiphout RGPM, Granton P et al. Radiomics: extracting more information from medical images using advanced feature analysis. *Eur J Cancer*. 2012;48(4):441–6.
3. Gillies RJ, Kinahan PE, Hricak H. Radiomics: images are more than pictures, they are data. *Radiology*. 2016;278(2):563–77.
4. Aerts HJWL, Velazquez ER, Leijenaar RTH, Parmar C, Grossmann P, Carvalho S et al. Decoding tumour phenotype by noninvasive imaging using a quantitative radiomics approach. *Nat Commun*. 2014;5(1):4006.
5. van Timmeren JE, Cester D, Tanadini-Lang S, Alkadhi H, Baessler B. Radiomics in medical imaging: “how-to” guide and critical reflection. *Insights Imaging*. 2020;11(1):91.
6. Traverso A, Wee L, Dekker A, Gillies R. Repeatability and reproducibility of radiomic features: a systematic review. *Int J Radiat Oncol Biol Phys*. 2018;102(4):1143–58.
7. Zwanenburg A, Vallières M, Abdalah MA, Aerts HJWL, Andrearczyk V, Apte A et al. The image biomarker standardization initiative: standardized quantitative radiomics for high-throughput image-based phenotyping. *Radiology*. 2020;295(2):328–38.
8. Camastra C, Pasini G, Stefano A, Russo G, Vescio B, Bini F et al. Development and implementation of an innovative framework for automated radiomics analysis in neuroimaging. *J Imaging*. 2024;10(4):96.
9. Nioche C, Orlhac F, Boughdad S, Reuzé S, Goya-Outi J, Robert C et al. LIFEx: a freeware for radiomic feature calculation in multimodality imaging to accelerate advances in the characterization of tumor heterogeneity. *Cancer Res*. 2018;78(16):4786–9.
10. Deasy JO, Blanco AI, Clark VH. CERR: a computational environment for radiotherapy research. *Med Phys*. 2003;30(5):979–85.
11. Hatt M, Cheze Le Rest C, Antonorsi N, Tixier F, Tankyevych O, Jaouen V et al. Radiomics in PET/CT: current status and future AI-based evolutions. *Semin Nucl Med*. 2021;51(2):126–33.
12. Rokuss M, Kovacs B, Kirchhoff Y, Xiao S, Ulrich C, Maier-Hein KH et al. From FDG to PSMA: a hitchhiker’s guide to multitracer, multicenter lesion segmentation in PET/CT imaging. *arXiv*: 2409.09478. 2024.
13. Wasserthal J, Breit HC, Meyer MT, Pradella M, Hinck D, Sauter AW et al. TotalSegmentator: robust segmentation of 104 anatomic structures in CT images. *Radiol Artif Intell*. 2023;5(5):e230024.
14. Ferrara D, Pires M, Gutschmayer S, Yu J, Abdelhafez YG, Abenavoli E et al. Sharing a whole-/total-body [18F]FDG-PET/CT dataset with CT-derived segmentations: an ENHANCE.PET initiative. *Res Sq*. 2025:rs.3.rs–7169062.
15. Sundar LKS, Yu J, Muzik O, Kulterer OC, Fueger B, Kifjak D et al. Fully automated, semantic segmentation of whole-body 18F-FDG PET/CT images based on data-centric artificial intelligence. *J Nucl Med*. 2022;63(12):1941–8.
16. Wahl RL, Jacene H, Kasamon Y, Lodge MA. From RECIST to PERCIST: evolving considerations for PET response criteria in solid tumors. *J Nucl Med*. 2009;50:122S–150S.
17. Vanderhoek M, Perlman SB, Jeraj R. Impact of the definition of peak standardized uptake value on quantification of treatment response. *J Nucl Med*. 2012;53(1):4–11.
18. Kido H, Kato S, Funahashi K, Shibuya K, Sasaki Y, Urita Y et al. The metabolic parameters based on volume in PET/CT are associated with clinicopathological N stage of colorectal cancer and can predict prognosis. *EJNMMI Res*. 2021;11(1):87.
19. Du S, Sun H, Gao S, Xin J, Lu Z. Metabolic parameters with different thresholds for evaluating tumor recurrence and their correlations with hematological parameters in

- locally advanced squamous cell cervical carcinoma: an observational ^{18}F -FDG PET/CT study. *Quant Imaging Med Surg.* 2019;9(3):440–52.
20. Im HJ, Bradshaw T, Solaiyappan M, Cho SY. Current methods to define metabolic tumor volume in positron emission tomography: which one is better? *Nucl Med Mol Imaging.* 2018;52(1):5–15.
 21. Boellaard R, Delgado-Bolton R, Oyen WJG, Giammarile F, Tatsch K, Eschner W et al. FDG PET/CT: EANM procedure guidelines for tumour imaging: version 2.0. *Eur J Nucl Med Mol Imaging.* 2015;42(2):328–54.
 22. Lorensen WE, Cline HE. Marching cubes: a high resolution 3D surface construction algorithm. *SIGGRAPH Comput Graph.* 1987;21(4):163–9.
 23. Cottreau AS, Nioche C, Dirand AS, Clerc J, Morschhauser F, Casasnovas O et al. ^{18}F -FDG PET dissemination features in diffuse large B-cell lymphoma are predictive of outcome. *J Nucl Med.* 2020;61(1):40–5.
 24. Förner L, Bäßler J, Sulski C, Enke J, Lapa C, Wendler T. Automated AI-based PET/CT analysis for monitoring immunotherapy response in metastatic melanoma. *Proc EANM.* 1:100004.

